Preclinical evaluation of [(18)F]PK-209, a new PET ligand for imaging the ion-channel site of NMDA receptors.

By Golla SS, Klein PJ, Bakker J, Schuit RC, Christiaans JA, van Geest L, Kooijman EJ, Oropeza-Seguias GM, Langermans JA, Leysen JE, Boellaard R, Windhorst AD, van Berckel BN, Metaxas A.

Published in Nucl Med Biol. 2015 Feb;42(2):205-12.
doi: 10.1016/j.nucmedbio.2014.09.006.

Preclinical evaluation of [^{18}F]PK-209, a new PET ligand for imaging the ion-channel site of NMDA receptors

Abbreviated title: PET imaging of NMDArs with [^{18}F]PK-209

Sandeep SV Golla[1], Pieter J Klein[1*], Jaco Bakker[2], Robert C Schuit[1], Johannes AM Christiaans[1], Leo van Geest[2], Esther JM Kooijman[1], Gisela M Oropeza-Seguias[1], Jan AM Langermans[2], Josée E Leysen[1], Ronald Boellaard[1], Albert D Windhorst[1], Bart NM van Berckel[1], Athanasios Metaxas[1]

*Equal contribution

[1]*Department of Radiology & Nuclear Medicine, Neuroscience Campus Amsterdam, VU University Medical Center, Amsterdam, the Netherlands*

[2]*Biomedical Primate Research Centre, Rijswijk, the Netherlands*

Corresponding author:
Athanasios Metaxas
VU University Medical Center (VUmc)
Department of Radiology & Nuclear Medicine, Neuroscience Campus Amsterdam
Location Radionuclide Center, De Boelelaan 1085 c
1081 HV Amsterdam
The Netherlands
Tel: +31 (0)20 4449704; Fax: +31 (0)20 4449121
Email: ametaxas@rnc.vu.nl; a.metaxas@hotmail.com

Keywords: PET, imaging, NMDA, ion-channel, brain, primate, *N*,*N*'-diaryl-*N*-methylguanidine, [^{18}F]PK-209.

Abstract

Introduction**:** The present study was designed to assess whether [^{18}F]PK-209 (3-(2-chloro-5-(methylthio)phenyl)-1-(3-([^{18}F]fluoromethoxy)phenyl)-1-methylguanidine) is a suitable ligand for imaging the ion-channel site of *N*-methyl-$_{D}$-aspartate receptors (NMDArs) using positron emission tomography (PET).

Methods**:** Dynamic PET scans were acquired from male rhesus monkeys over 120 min, at baseline and after the acute administration of dizocilpine (MK-801, 0.3 mg/kg; n=3/condition). Continuous and discrete arterial blood samples were manually obtained, to generate metabolite-corrected input functions. Parametric volume-of-distribution (V_T) images were obtained using Logan analysis. The selectivity profile of PK-209 was assessed *in vitro*, on a broad screen of 79 targets.

Results: PK-209 was at least 50-fold more selective for NMDArs over all other targets examined. At baseline, prolonged retention of radioactivity was observed in NMDAr-rich cortical regions relative to the cerebellum. Pretreatment with MK-801 reduced the V_T of [^{18}F]PK-209 compared with baseline in two of three subjects. The rate of radioligand metabolism was high, both at baseline and after MK-801 administration.

Conclusions**:** PK-209 targets the intrachannel site with high selectivity. Imaging of the NMDAr is feasible with [^{18}F]PK-209, despite its fast metabolism. Further *in vivo* evaluation in humans is warranted.

1. Introduction

N-methyl-$_D$-aspartate receptors (NMDArs) are glutamate-gated cation channels with key physiological roles in the developing and adult brain. Their timely activation is required for synaptic maturation and plasticity, underlying mental processes as essential for life as memory and learning [1]. The aberrant activation of NMDArs, however, can have devastating effects on neuronal survival and physiological brain function. NMDAr overactivation is known to promote cell death by excitotoxicity [2], a process that has been implicated in the pathogenic mechanisms of ischaemia, epilepsy and chronic neurodegenerative disorder, including Alzheimer's, Parkinson's and Huntington's diseases [3]. NMDAr hypofunction, on the other hand, has been linked to the pathophysiology of schizophrenia and autism spectrum disorder [4], and may be related with increased risk for drug abuse [5]. Because of the substantial roles of NMDArs in health and disease, there is considerable interest in developing an imaging tool to assess the functional state of the NMDAr *in vivo*, both for diagnostic and research purposes.

The activation of NMDArs is controlled by multiple endogenous ligands, which tightly regulate the probability of ion-channel opening by binding to distinct sites on the receptor [6]. There are at least six different binding sites on the NMDArs, including recognition sites for the agonist glutamate, the co-agonists glycine and serine, as well as for ligands that modulate receptor function, such as polyamines, metal ions and protons. Of the multiple binding sites, the one that is located within the pore of the ion-channel is an attractive target for examining the functional state of NMDArs. Due to its unique physical location, the ion-channel site is primarily accessible when the NMDAr is in an open conformation, i.e. activated by glutamate and glycine [7]. Thus, the *in vivo* uptake of radiotracers targeting the intrachannel site is likely

to be proportional to the amount of activated NMDArs, and could be used to determine their functional state and brain regional distribution [8].

Although there have been several attempts to label the ion-channel site using Positron Emission Tomography (PET), the majority of efforts has been confounded by poor radiotracer selectivity and affinity, low brain entrance, rapid radioligand metabolism, and/or inability to establish specific NMDAr targeting *in vivo* [9-**10**]. We have previously described the synthesis, radiosynthesis, *in vitro* and *ex vivo* evaluation of a series of *N*,*N*'-diaryl-*N*-methylguanidines, targeting the NMDAr ion-channel site [11]. In that series, [^{18}F]PK-209 (Figure 1) was the most promising candidate ligand for imaging NMDArs. The compound had an apparent affinity value of 18 nM against [^{3}H]MK-801 (Ki) and a distribution coefficient value of 1.45 ($LogD_{oct,7.4}$), indicating high affinity for the NMDAr and moderate lipophilicity, respectively. In biodistribution experiments in mice, the forebrain-to-cerebellum ratio of radioactivity uptake after the administration of [^{18}F]PK-209 was in excess of 1.7, indicating accumulation of the tracer in NMDAr-rich brain regions. Importantly, *ex vivo* autoradiography showed that the brain uptake of [^{18}F]PK-209 was reduced by up to 30% from control levels after the acute administration of dizocilpine (MK-801; 0.6 mg/kg, intraperitoneally), indicating selectivity of the radioligand for the NMDAr ion-channel site. In the present study, we report on a comprehensive pharmacological selectivity profile for PK-209, and examine whether selective labeling and quantification of the NMDA receptor ion-channel is feasible in the nonhuman primate brain using [^{18}F]PK-209 PET.

2. Materials and Methods

2.1 Selectivity profile of PK-209

The pharmacological selectivity of PK-209 was evaluated at Cerep (Poitiers, France). A single concentration of PK-209 (10 μM) was initially screened on a panel of 79 targets, comprising neurotransmitter receptors and transporters, and ion-channels (Supplementary Table 1). A percent (%) inhibition of control specific binding, obtained in the presence of 10 μM PK-209, was calculated for each target. The affinity of PK-209 for targets showing ≥50% inhibition of control specific binding in the primary screen was subsequently derived from full concentration-response inhibition curves, which were obtained using 8 concentrations of PK-209. Hill coefficients (nH) and IC_{50} values from the competition binding experiments were derived by non-linear regression analysis. IC_{50} values were converted to inhibition constants (Ki values) using the Cheng and Prusoff equation for binding assays: $Ki=IC_{50}/(1+L/K_D)$, where L is radioligand concentration in the assay and K_D the affinity of the radioligand for its corresponding target. The K_D values of the reference radioligands were obtained in saturation experiments, which were run in parallel to the competition binding studies. Details of the Cerep selectivity assays are available from www.cerep.fr.

2.2 **Radiotracer** preparation

The precursor synthesis [12] and radiolabeling procedures [13] for [^{18}F]PK-209 have been described previously. The radiotracer was formulated in a phosphate-buffered saline solution containing 8.6% ethanol, and administered by intravenous injection of ≤10 mL. For baseline studies, injected activity was 138.8±30.4 MBq and specific activity 135.8±15.4 GBq/μmol, corrected to scan acquisition time. For blocking studies, injected activity and specific activity at scan acquisition time were 124.7±19.5 MBq and 97.2±24.4 GBq/μmol, respectively. In all cases, synthesis time including HPLC purification was ≈90 min, and radiochemical purity of the final product >98%.

2.3 Subjects, anaesthesia and treatment

All experimental procedures complied with European Commission Directive 2010/63/EU, regulating animal research, and were approved by the independent Animal Experimental Committee of the Biomedical Primate Research Centre in Rijswijk, the Netherlands (BPRC; DEC#717BPRC).

Three adult male rhesus monkeys (*Macaca mulatta*) were included in the study, aged 17-19 years and weighing 7.6-13.5 kg. Monkeys were group-housed at the BPRC, in an enriched, temperature-controlled environment (20-22°C), under a 12 h light/dark circadian cycle. The animals were maintained on a standard monkey pellet diet (Ssniff®, Soest, Germany) supplemented with vegetable and fresh fruit, and were fasted for a period of 16 h prior to anaesthesia. Drinking water was available *ad libitum*. All animals had received a comprehensive physical, haematological and biochemical examination prior to study initiation and remained under constant veterinary supervision throughout the experiments.

On the day of each baseline scan, monkeys were transported from the BPRC in Rijswijk to the Radionuclide Center in Amsterdam (RNC, Amsterdam, the Netherlands). The animals were trained to voluntary enter their transit cages, and no anaesthesia was used during the 40 min transportation period. At the RNC, monkeys were sedated with an injection of medetomidine hydrochloride (60 μg/kg; Sedastart 1 mg/mL, AST Farma BV, Oudewater, the Netherlands) and midazolam (0.3 mg/kg; Midazolam Actavis 5 mg/mL; Actavis BV, Baarn, the Netherlands), which were administered intramuscularly (IM). Immobilized animals were brought into the imaging facilities, and placed on a warm Harvard blanket in order to maintain normothermia (Homeothermic Blanket 60x90cm, Harvard Apparatus GmbH, March-Hugstetten, Germany). The cephalic veins of both arms were catheterized with a Vasofix®

Braunüle® catheter (B. Braun Melsungen AG, Germany). The left cephalic line was used for the induction and maintenance of propofol anesthesia, which was delivered at a rate of 0.2 mg/kg/min (PropoVet Multidose 10 mg/mL, Fresenius Kabi AB, Uppsala, Sweden). The right cephalic line was used to infuse NaCl/glucose, at a rate of 1 mL/kg/h (0.45% Sodium chloride & 2.5% Glucose 500ML, Baxter BV, Utrecht, the Netherlands). For endotracheal intubation, xylocaine 10% was sprayed into the larynx and trachea (AstraZeneca BV, Zoetermeer, the Netherlands). The monkeys were subsequently positioned in the scanner in the supine position, with their head fixed at the appropriate orientation within the field of view, using custom-built face masks. Haemoglobin oxygen saturation levels (SpO2) and heart rate were continuously measured with a Mindray monitor (PM-8000, GmbH, Hamburg, Germany). Body temperature was continuously monitored with a rectal probe (PM-8000, GmbH, Hamburg, Germany). At the end of each scan, and following recovery from immobilization, animals were transported from the RNC in Amsterdam to the BPRC in Rijswijk. Full recovery from anaesthesia was defined as the animal's ability to be safely reunited with its home-cage companions, after walking and climbing confidently in the transit cage [14].

Blocking scans were performed one week after baseline for subjects 1 and 2, and two weeks after baseline for subject 3, according to the above described protocol. (+)-MK-801 hydrogen maleate was used to block NMDArs (Sigma Aldrich, Zwijndrecht, the Netherlands). The drug was administered via the right cephalic vein, 30 min prior to radiotracer injection, at a dose of 0.3 mg/kg (free-base weight). The blocking dose and timing of MK-801 administration were based on glutamate microdialysis studies in the rhesus monkey [15], and were chosen to avoid alterations in extracellular levels of glutamate following NMDAr antagonism.

2.4 Image acquisition

Magnetic Resonance Imaging (MRI) data were acquired prior to the PET studies, using a 3 Tesla Siemens Trio scanner (Siemens, Erlangen, Germany), and a standard T1-weighted 3D MPRAGE sequence (TR 2300 ms, TI 1100 ms, TE 3.93 ms, 192 sagittal slices, field of view 256 mm). All images were reconstructed into a matrix of 192 × 256 × 256 voxels, with a voxel size of 1.0×1.0×1.0 mm.

PET measurements were performed on a Siemens ECAT HRRT scanner, operated in 3D mode (CTI/Siemens, Knoxville, TN, USA). A detailed description of the HRRT scanner, its reconstruction software and performance has been reported previously [16]. For attenuation and scatter correction, each PET scan was preceded by a 6 min transmission scan, which was performed using a 740 MBq ^{137}Cs (662 keV) rotating point source. Dynamic PET scans were acquired over 120 min **(frame end time)**, starting simultaneously with a bolus injection of [^{18}F]PK-209 into the right cephalic vein. Data were stored in 64-bit list mode format and subsequently binned into 20 time frames. Frame sequence definition was 6x10s, 2x30s, 3x60s, 2x150s, 2x300s, 2x600s, 2x1200s, and 1x2400s. Reconstruction was performed using the ordered subsets weighted, least-squares algorithm. All data were normalized and corrected for scatter, random coincidences, attenuation, decay and dead time. All images were reconstructed into a matrix of 256 × 256 × 207 voxels, with a voxel size of 1.218 × 1.218 × 1.218 mm.

2.5 Blood sampling and metabolite analysis

Blood was manually sampled from the femoral artery using a 20G Vacuette (Vacuette 20G x 1 ½"; Greiner Bio-One GmbH, Kremsmünster, Austria), collected into heparin tubes (Greiner Bio-One GmbH, Kremsmünster, Austria), and mixed by inversion. Sampling began simultaneously with an injection of [^{18}F]PK-209, and continued for a period of 5 min, at 5-10 s intervals. Radioactivity in 100 µL aliquots of whole-blood was directly measured in a

Wallac 2480 Wizard^2 Automatic Gamma Counter (PerkinElmer, Groningen, the Netherlands). Discrete blood samples were collected at 5, 10, 15, 30, 60, 90 and 120 min post-injection, to measure plasma and whole-blood ratios, calibrate the whole-blood data, and determine metabolite fractions.

For metabolite analysis, blood samples were centrifuged at 4 000 rpm for 5 min at 4°C, in a Hettich Universal 16 table centrifuge (Hettich Benelux BV, Geldermalsen, the Netherlands). Plasma was separated from blood cells and loaded onto an activated tC2 Sep-Pak cartridge (Waters, Etten-Leur, the Netherlands), which was washed with 3 mL of demineralised (demi) water. The eluate was defined as the polar radiolabeled metabolite fraction. The tC2 Sep-Pak was then washed with 2 mL of methanol and 1 mL of demi water. This eluate was defined as the non-polar fraction, and analyzed using reverse phase HPLC [Dionex Ultimate 3000 HPLC system, equipped with a Phenomenex Gemini C18 5µm 250 x 10.0 mm column, using a gradient of 50 mM $NH_4H_2PO_4$ / acetonitrile (80/20 to 30/70, v/v) in 12.5 minutes at a flow rate of 3.0 mL/min]. Radioactivity in polar and non-polar fractions was measured off-line in a Wallac 2480 Wizard^2 Automatic Gamma Counter (PerkinElmer, Groningen, the Netherlands).

2.6 Image processing

MRI and PET images were coregistered using the software package VINCI [17]. Individualized, whole-brain masks were manually drawn for each averaged PET image (frames 5-16) and for the MRI image of each subject, to ensure coregistration based on brain voxels only. Regions-of-interest (ROIs) were automatically delineated onto coregistered MRI scans using the INIA19 template for the rhesus monkey brain [18]. The following regions were defined for the left and right hemispheres: frontal lobe, temporal lobe, occipital lobe, striatum (caudate and putamen), and cerebellum. Whole-brain gray matter voxels were also

included. ROIs were projected onto the complete dynamic PET images to extract the corresponding time-activity curves, using in-house software written in MATLAB® (R2007b, The MathWorks, Natick, MA, USA). The arterial plasma input function was derived from continuous and discrete blood samples, which were corrected for parent fraction, whole blood/plasma ratio and delay. The 1 minus polar fraction was used as a surrogate of unmetabolized [^{18}F]PK-209. Parametric volume-of-distribution (V_T) images were used to evaluate the V_T of [^{18}F]PK-209 at baseline conditions and following the administration of MK-801. Images were generated using plasma-input Logan analysis [19].

2.7 Data analysis and statistics

Radioactivity concentration was expressed as percentage of injected dose per cm^3 of brain tissue (%ID/cm^3). Area under the time-activity curves ($AUC_{0\text{-}100.5}$; **frame midpoint times**) was calculated as a simplified measurement of accumulated brain uptake of [^{18}F]PK-209-derived radioactivity. The between-subjects coefficient of variation (CV) was calculated as the ratio of standard deviation to mean V_T values. The systemic clearance of [^{18}F]PK-209 was calculated as injected activity, divided by area under the arterial plasma concentration curve (extrapolated to infinity). Non-parametric statistics were used to analyse all data sets. Friedman tests (χ^2) for the factors brain region and treatment were used to compare mean V_T values of [^{18}F]PK-209 between baseline and blocking conditions in individual brain areas. Wilcoxon matched-pairs tests (Z) were used to compare the overall V_T of [^{18}F]PK-209 before and after the administration of MK-801, at the within-subject level. Where applicable, results are presented as mean ± standard error of the mean (SEM).

3. Results

3.1 *In vitro* pharmacological selectivity profile of PK-209

At a concentration of 10 μM, PK-209 showed no significant binding to 70 of the 79 targets tested. Affinity values for targets showing ≥50% inhibition of control specific binding in the primary screen are listed in Table 1. PK-209 exhibited >50-fold selectivity for the ion-channel of NMDArs over all other targets examined.

3.2 Physiological response to anaesthesia

The sedative effect of medetomidine/midazolam occurred without excitation. Immobilization was induced within 10-15 min of drug administration for all subjects. Animals were breathing spontaneously under propofol anaesthesia, at a stable rate of 30-40 breaths/min. Percent oxygen saturation (>95%) and heart rate (120-160 beats/min) were not suppressed during the baseline or blocking scans. Body temperature decreased gradually during both baseline and blocking experiments, from 37.5-38.0°C to 34.5-35.5°C. Full recovery from anaesthesia occurred within 4 h of propofol cessation on the day of the baseline scans. Return to pre-anaesthetic condition was prolonged to >8 h by the administration of MK-801. Recovery from anaesthesia was uneventful for subjects 1 and 2. Subject 3 showed symptoms of general discomfort, lacrimation, agitation, and loss of appetite following its baseline scan. The animal responded to three days of treatment with buprenorphine (0.02 mg/kg, twice daily, IM) and meloxicam (0.10 mg/kg, once daily, per os), and was scanned healthy 2 weeks after baseline.

3.3 Metabolism of [^{18}F]PK-209

Figure 2 shows mean fractions in the plasma of unchanged [^{18}F]PK-209 and its metabolites as a function of time. 10 min after the administration of [^{18}F]PK-209, 60±4% of total radioactivity in plasma was due to polar metabolites. HPLC analysis of the non-polar fraction at the 10 min time-point demonstrated that unchanged [^{18}F]PK-209 and 1 major metabolite accounted for 30±6% and 8±3% of total plasma radioactivity, respectively. Retention times

were 12.6 min for [^{18}F]PK-209 and 10.1 min for the more-polar metabolite. The recovery of radioactivity off the HPLC was >97% over a 15 min run. The mean percentage of plasma radioactivity attributable to non-metabolised tracer throughout the 2 h studies was 19.2±0.5%, while polar and non-polar metabolites of [^{18}F]PK-209 accounted for 75.0±0.5% and 5.7±0.1% of the overall plasma radioactivity, respectively. No radioactivity uptake was observed in the jaw and skull in the dynamic PET images (supplementary Figure 1). Wilcoxon matched-pairs tests were used to compare parent and metabolite fractions of radioactivity between baseline and blocking scans at individual time-points. There was no effect of MK-801 administration on the metabolism of [^{18}F]PK-209 (P>0.05 for each time-point).

3.4 Pharmacokinetics of [^{18}F]PK-209

The parent plasma input function peaked at 37.8±4.2 s post-injection, and decreased to 10% of its peak value within 3 min (Figure 3). The mean area under the input function curve was 20.6±6.6 MBq/mL·min and 18.3±4.6 MBq/mL·min for the baseline and blocking conditions, respectively (Z=0.0, P>0.05). Under both conditions, plasma to whole-blood radioactivity ratios ranged from 1.0±0.1 at 5 min post-injection, to 1.2±0.0 at 30 min, remaining stable thereafter until completion of the 2 h scans. The terminal plasma clearance of [^{18}F]PK-209 was 6.6±0.5 mL/min at baseline, and did not change after treatment with MK-801 (6.8±0.4 mL/min; Z=0.0, P>0.05).

3.5 Regional distribution of radioactivity and time-activity curves (TACs), at baseline and after MK-801 treatment

Figure 4 shows TACs of all ROIs examined under baseline and blocking conditions. Uptake in the whole-brain peaked at 16.3±1.7 min during the baseline scans, and was equivalent to 0.029±0.002 %ID/cm^3. The rank order of peak radioactivity concentration (%ID/cm^3) was

striatum (0.036±0.004) = cerebellum (0.036±0.005) > occipital (0.033±0.004), temporal (0.029±0.001), and frontal lobes (0.028±0.001). The washout of [^{18}F]PK-209-derived radioactivity varied between brain regions. Concentrations at 100.5 min declined to 37.2±5.0% of the peak value in the cerebellum, to 45.3±5.3% in the striatum, and to 61.7±6.5% in the frontal lobe. The mean area under the TACs ($AUC_{0\text{-}100.5}$) of all regions analysed was 2.31±0.07 %ID/cm^3·min for the baseline condition.

Treatment with MK-801 30 min before the administration of [^{18}F]PK-209 decreased the mean $AUC_{0\text{-}100.5}$ to 1.97±0.04 %ID/cm^3·min, representing a reduction of 14.7% from baseline [$\chi^2_{(9)}$=14.8, P=0.09]. The decrease in uptake was noticeable in all ROIs during the washout phase of the blocking scans, from 20-100.5 min after the administration of [^{18}F]PK-209. The regional rank order and peak values of radioactivity concentration were unaltered by the administration of MK-801 [$\chi^2_{(9)}$=16.6, P>0.05]. Peak uptake values, however, were observed earlier than baseline during the blocking scans [$\chi^2_{(9)}$=19.6, P<0.05; Friedman test]. For the whole-brain, radioactivity uptake under blocking conditions peaked at 8.8±2.6 min, and was equivalent to 0.029±0.001 %ID/cm^3.

3.6 Effect of MK-801 administration on the V_T of [^{18}F]PK-209

Table 2 shows individual V_T values of [^{18}F]PK-209 for all ROIs examined, at baseline and after MK-801 administration. Parametric images were obtained by plasma-input Logan analysis and are shown for subject 1 in Figure 5a. The rank order of regional V_T values (mL/cm^3) at baseline was striatum (12.9±1.2) and cerebellum (11.5±1.0) > temporal (10.9±0.4), occipital (10.9±1.2), and frontal lobes (10.5±0.8). Between-subject variability in quantifying the V_T of [^{18}F]PK-209 ranged from 19.0% in the occipital, to 8.9% in the frontal lobe.

Mean V_T values in all brain areas analysed decreased from 11.3±0.4 mL/cm^3 at baseline to 9.7±0.8 mL/cm^3 after MK-801 administration [$\chi^2_{(9)}$=11.4, P>0.05; Friedman test]. The effect of pretreatment with MK-801 on the V_T of [^{18}F]PK-209 varied between subjects. Brain regional V_T values were overall reduced compared with baseline for subjects 1 and 2 (Z=2.0, P<0.05), and increased for subject 3 (Z=2.0, P<0.05). In all cases, Logan plots became linear from 10 min post injection of [^{18}F]PK-209 (t*=10 min; Figure 5b).

4. Discussion

The present study was designed to evaluate whether [^{18}F]PK-209 is a suitable tracer for imaging the ion-channel site of NMDArs. We show that PK-209 targets the intrachannel site with high apparent affinity and selectivity, and provide evidence that PET-measurable quantification of the NMDAr is feasible in the rhesus monkey brain using [^{18}F]PK-209.

Only a limited number of ion-channel radiotracers have been tested for their ability to visualize NMDArs in the nonhuman primate brain [9-10]. These include radiolabeled analogues of MK-801, tenocyclidine (TCP), ketamine, memantine, and the guanidine GMOM, a ligand that has been labeled with carbon-11 and is structurally closely related with PK-209 [20]. The radiochemical synthesis advantages of [^{18}F]PK-209 over **[^{11}C]GMOM** range from suitability of labeling PK-209 with fluorine-18, to rapidly delivering [^{18}F]PK-209 in adequate radiochemical yields (>20%, decay-corrected) and with high specific activity (≈100 GBq/μmol). From a pharmacological perspective, the minimal off-target effects observed on a broad selectivity screen render PK-209 one of the most selective ligands available to date for the ion-channel site of NMDArs. The compound's selectivity profile is comparable with that of the reference standard for non-competitive NMDAr antagonism, MK-801 [21]. In addition, the commercially obtained apparent affinity value for PK-209 (Ki=22 nM) is in the range previously reported by our group (Ki=18 nM), confirming the ligand's

high affinity for the intrachannel site of NMDArs [12]. Taken together, these *in vitro* results suggest that contrary to ^{18}F-labeled derivatives of MK-801 [22], TCP [23] or memantine [24], the use of [^{18}F]PK-209 for PET imaging of the NMDAr is unlikely to be limited by poor tracer selectivity and/or potency.

The rate of [^{18}F]PK-209 metabolism was high in the monkey plasma, and similar to that reported for enantiomers of [^{11}C]ketamine [25] and [^{11}C]GMOM [20]. 10 min following [^{18}F]PK-209 administration, the percentage of plasma radioactivity attributable to unchanged tracer was already less than 50%, indicating that rapid metabolism hinders prolonged measurements of [^{18}F]PK-209 from arterial plasma. To reduce uncertainty in determining the plasma concentration of [^{18}F]PK-209, particularly during later time frames, the 1 minus polar radioactivity fraction was used as a surrogate of non-metabolised radiotracer. Two assumptions were accepted in taking this approach, namely that polar metabolites of [^{18}F]PK-209 do not cross the blood-brain barrier, and that the accumulation of lipophilic metabolites of [^{18}F]PK-209 in the monkey brain is low, if any at all. Using an identical method of analysis as in the present report [11], we have previously shown that polar metabolites of [^{18}F]PK-209 hardly enter the mouse brain (≈4% contribution to total brain radioactivity, 60 min after radioligand injection). Since over the 2 h course of these scans 75.0% and 19.2% of plasma radioactivity was associated with polar metabolites and parent tracer, respectively, a potential contribution of lipophilic metabolites to the PET signal of [^{18}F]PK-209 is indeed expected to be low. The reversible apparent kinetics in the TACs, and the fact that linearity was attained from early to late time-points in the Logan plots, further argue against the significant accumulation of [^{18}F]PK-209-derived metabolites in the rhesus brain.

[^{18}F]PK-209 entered the brain readily, showing a fairly uniform distribution in the brain areas examined, namely between the cortex, striatum and the cerebellum. Due to the low signal-to-noise ratio in the dynamic PET images, and in order to perform a user-independent analysis, small ROIs were not delineated in the current study. Instead, the uptake of [^{18}F]PK-209 was quantified in large brain areas, which are known to exhibit high (cortex), moderate (striatum) and low (cerebellum) levels of NMDAr expression, *in vitro* [26]. The regional variation of V_T estimates at baseline was <20%, indicating acceptable between-subject variability in quantifying the uptake of [^{18}F]PK-209 using Logan plots. In addition, prolonged retention of radioactivity during the baseline scans was clearly observed in NMDAr-rich regions relative to the cerebellum, suggesting specific receptor targeting. However, the rank order of regional [^{18}F]PK-209 distribution was at odds with the rank order of NMDAr density predicted from *in vitro* studies, since higher V_T values were observed in the striatum and the cerebellum rather than the cortex.

The discrepancy between the *in vitro* and PET-measurable distribution of NMDArs has been repeatedly noted in the literature [22, 24, 27-28]. Perhaps the most convincing explanation hypothesized to account for the discrepant observations relates to the state of NMDAr activation. The *in vitro* preparations used to visualize the localisation of NMDArs are likely to contain concentrations of endogenous agonists that are high enough to fully activate the receptors. This is evident from autoradiographic experiments, in which exogenously applied glutamate and glycine do not enhance the binding of [^{3}H]MK-801 to NMDArs above baseline levels [29-30]. Since access to the ion-channel site depends on the concentration of glutamate and glycine [7], the *in vitro* binding of radioligands to maximally activated receptors may not necessarily reflect their *in vivo* uptake, and thus correspond to the PET-measurable distribution of NMDArs. In addition, limited access to the intrachannel site in the living brain

can be anticipated under physiological conditions, since NMDAr overactivation has been associated with several pathological processes. Further explanations for the discrepancies in NMDAr distribution between *in vitro* and imaging studies may include differences in ion-channel opening times between brain regions [31], which can only influence the uptake of radioligands *in vivo*, the presence of two binding sites within the ion-channel of NMDArs [32], which might be differentially available between *in vitro* and *in vivo* conditions [33], and - less likely - differences in regional NMDAr expression between rodent and primate species. In any case, the pattern of NMDAr distribution in the rhesus brain is consistent with that observed in humans, using ion-channel tracers such as [^{123}I]CNS1261 [34] or [^{18}F]GE-179 [28]. Hence, our results confirm the discrepancies between the *in vitro* and imaging experiments, and invite further consideration of the mechanisms that may give rise to them.

Pretreatment with MK-801 30 min before the administration of [^{18}F]PK-209 shifted the peak of the time-activity curves to the left compared with baseline, without altering the maximum radioactivity concentration values. The increased uptake of radioactivity during the initial time frames of the blocking scans could be related to MK-801-induced increases in regional cerebral blood flow [35], suggesting that the distribution of [^{18}F]PK-209 may be partially perfusion-dependent. However, since there was no change in the peak amplitude of radioactivity concentrations compared with baseline, a contribution of tracer efflux to the shape of the time-activity curves, alone or in combination with other kinetic parameters, cannot be excluded. While these observations require further investigation, the Logan plot analysis we employed provides an estimate of V_T at equilibrium that is perfusion-independent, suggesting that possible MK-801-induced alterations in cerebral blood flow are unlikely to have influenced the V_T values of [^{18}F]PK-209 under blocking conditions. In support of this suggestion, leftward shifts in uptake were consistently observed during the blocking scans,

while the effect of pretreatment with MK-801 on the V_T of [^{18}F]PK-209 varied between subjects.

Logan-derived V_T was overall decreased compared with baseline for subjects 1 and 2, and increased for subject 3. It is unlikely that these changes are secondary to MK-801-induced alterations in the peripheral pharmacokinetics of [^{18}F]PK-209, since the profile of metabolite formation, the distribution between plasma and whole-blood, the arterial plasma concentration, and the clearance of [^{18}F]PK-209 at baseline were unaffected by the administration of MK-801. Moreover, while binding to plasma proteins was not measured in this study, it is unclear how pretreatment with MK-801 may both have increased and decreased the plasma-free concentration of [^{18}F]PK-209, leading to inconsistent alterations in its V_T compared with baseline. Therefore, the effects of MK-801 administration on the uptake of [^{18}F]PK-209 are probably due to pharmacodynamic, rather than pharmacokinetic reasons. To the best of our knowledge, this is the first nonhuman primate study to demonstrate decreases in the V_T of an intrachannel PET tracer following the administration of the highly selective ion-channel blocker MK-801, suggesting that [^{18}F]PK-209 can visualize and quantify the NMDAr *in vivo*. Nevertheless, a note of caution should be inserted in interpreting the results of the blocking scans, since the reason for increased V_T values in subject 3 is unknown.

One possible explanation may involve alterations in the target of interest itself, i.e. changes in the functional state of NMDArs, which may have occurred in the interval between the baseline and blocking scans of subject 3. Following its baseline scan, subject 3 was administered for 3 days with the partial μ-opioid receptor (MOP) agonist buprenorphine, for welfare reasons (0.02 mg/kg, twice daily). Agonists and partial agonists at the MOP, however,

are known to increase the function of NMDArs [36], in brain regions where the two receptors colocalise and may physically interact, including the striatum, cortex, and - to a smaller extent - the cerebellum [37]. Moreover, it is relatively well-established that the potentiating effects of MOP agonism on the function of NMDArs persist long after the end of opioid administration, both at the neurochemical and behavioural levels. For example, the binding of [^{3}H]MK-801 is increased in the brain of rats that have been withdrawn from treatment with partial MOP agonists [38], while the persistent functional potentiation of NMDArs plays a central role in opioid-induced analgesic tolerance and physical dependence [39]. Therefore, the increase in the V_T of [^{18}F]PK-209 in the buprenorphine-treated subject may be associated with opioid-induced increases in NMDAr function. In support of this suggestion, confounding effects of MOP agonism on blocking the uptake of 'state-dependent' NMDAr tracers have been documented previously in fentanyl-anaesthetized mice [40]. In addition, the relatively low blocking dose of MK-801 used in the present study is unlikely to have produced free brain concentrations of the drug that are high enough to occupy the entire population of NMDArs, thereby compensating for any potential increases in the receptor's function after the administration of buprenorphine [41]. Thus, it is intriguing to speculate that the increased uptake of [^{18}F]PK-209 compared with baseline in subject 3 may actually reflect the radioligand's ability to quantify alterations in the functional state of NMDArs.

Conclusions

PK-209 binds to the ion-channel site of NMDArs with high apparent affinity and selectivity. Although the rate of metabolism is high, the regional V_T of [^{18}F]PK-209 can be quantified in the primate brain with acceptable between-subject variability. Evidence for specific targeting of the NMDArs *in vivo* is modest but present in the current study, both at baseline and after the administration of MK-801. Further evaluation of [^{18}F]PK-209 in humans is warranted.

5. Acknowledgements

This work was supported by the Center for Translational Molecular Medicine (http://www.ctmm.nl), project LeARN (02N-101). Part of the work was also supported by the European Union's Seventh Framework Programme (FP7/2007-2013), grant agreement n° HEALTH-F2-2011-278850 (INMiND).

We thank Rolph van Kooij for his technical assistance in preparing [^{18}F]PK-209 and the staff of BV Cyclotron VU, Amsterdam, for supplying ^{18}F. We are grateful to Inge de Greeuw and Mariska Verlaan for their assistance in operating the HRRT scanner.

6. References

1. Paoletti P, Bellone C, Zhou Q. NMDA receptor subunit diversity: impact on receptor properties, synaptic plasticity and disease. Nat Rev Neurosci 2013; 14:383-400.

2. Olney JW. Excitotoxicity, apoptosis and neuropsychiatric disorders. Curr Opin Pharmacol 2003; 3:101-109.

3. Parsons MP, Raymond LA. Extrasynaptic NMDA receptor involvement in central nervous system disorders. Neuron 2014; 82:279-293.

4. Tarabeux J, Kebir O, Gauthier J, Hamdan FF, Xiong L, Piton A, et al. Rare mutations in N-methyl-D-aspartate glutamate receptors in autism spectrum disorders and schizophrenia. Transl Psychiatry 2011; 1:e55.

5. Madsen HB, Brown RM, Lawrence AJ. Neuroplasticity in addiction: cellular and transcriptional perspectives. Front Mol Neurosci 2012; 5:99.

6. Gonda X. Basic pharmacology of NMDA receptors. Curr Pharm Des 2012; 18:1558-1567.

7. Javitt DC, Zukin SR. Biexponential kinetics of [3H]MK-801 binding: evidence for access to closed and open N-methyl-D-aspartate receptor channels. Mol Pharmacol 1989; 35:387-393.

8. Waterhouse RN. Imaging the PCP site of the NMDA ion channel. Nucl Med Biol 2003; 30:869-878.

9. Sobrio F, Gilbert G, Perrio C, Barre L, Debruyne D. PET and SPECT imaging of the NMDA receptor system: an overview of radiotracer development. Mini Rev Med Chem 2010; 10:870-886.

10. Sobrio F. Radiosynthesis of carbon-11 and fluorine-18 labelled radiotracers to image the ionotropic and metabotropic glutamate receptors. J Labelled Comp Radiopharm 2013; 56:180-186.

11. Klein PJ, Christiaans JAM, Metaxas A, Schuit RC, Lammertsma AA, van Berckel BNM, et al. Synthesis, Structure Activity Relationship, Radiolabelling and Preclinical Evaluation of High Affinity Ligands for the Ion Channel of the N-Methyl-D-Aspartate Receptor as Potential Imaging Probes for Positron Emission Tomography. 2014; Submitted.

12. Klein PJ, Christiaans JAM, Metaxas A, Lammertsma AA, van Berckel BNM, Windhorst AD. Novel Radiotracer Development Poster Abstracts. J Cereb Blood Flow Metab 2012; 32:S100-S127.

13. Klein PJ, Metaxas A, Windhorst AD, Christiaans JAM, van Berckel BNM. N,n-substituted guanidine compound. Patent 2012; WO2012165956A1.

14. Bakker J, Thuesen LR, Braskamp G, Skaanild MT, Ouwerling B, Langermans JA, et al. Single subcutaneous dosing of cefovecin in rhesus monkeys (Macaca mulatta): a pharmacokinetic study. J Vet Pharmacol Ther 2011; 34:464-468.

15. Tsukada H, Nishiyama S, Fukumoto D, Sato K, Kakiuchi T, Domino EF. Chronic NMDA antagonism impairs working memory, decreases extracellular dopamine, and increases D1 receptor binding in prefrontal cortex of conscious monkeys. Neuropsychopharmacology 2005; 30:1861-1869.

16. de Jong HW, van Velden FH, Kloet RW, Buijs FL, Boellaard R, Lammertsma AA. Performance evaluation of the ECAT HRRT: an LSO-LYSO double layer high resolution, high sensitivity scanner. Phys Med Biol 2007; 52:1505-1526.

17. Cizek J, Herholz K, Vollmar S, Schrader R, Klein J, Heiss WD. Fast and robust registration of PET and MR images of human brain. NeuroImage 2004; 22:434-442.

18. Rohlfing T, Kroenke CD, Sullivan EV, Dubach MF, Bowden DM, Grant KA, et al. The INIA19 Template and NeuroMaps Atlas for Primate Brain Image Parcellation and Spatial Normalization. Front Neuroinform 2012; 6:27.

19. Logan J. Graphical analysis of PET data applied to reversible and irreversible tracers. Nucl Med Biol 2000; 27:661-670.

20. Waterhouse RN, Slifstein M, Dumont F, Zhao J, Chang RC, Sudo Y, et al. In vivo evaluation of [11C]N-(2-chloro-5-thiomethylphenyl)-N'-(3-methoxy-phenyl)-N'-methylguanid ine ([11C]GMOM) as a potential PET radiotracer for the PCP/NMDA receptor. Nucl Med Biol 2004; 31:939-948.

21. Wong EH, Kemp JA, Priestley T, Knight AR, Woodruff GN, Iversen LL. The anticonvulsant MK-801 is a potent N-methyl-D-aspartate antagonist. Proc Natl Acad Sci U S A 1986; 83:7104-7108.

22. Blin J, Denis A, Yamaguchi T, Crouzel C, MacKenzie ET, Baron JC. PET studies of [18F]methyl-MK-801, a potential NMDA receptor complex radioligand. Neurosci Lett 1991; 121:183-186.

23. Ouyang X, Mukherjee J, Yang ZY. Synthesis, radiosynthesis, and biological evaluation of fluorinated thienylcyclohexyl piperidine derivatives as potential radiotracers for the NMDA receptor-linked calcium ionophore. Nucl Med Biol 1996; 23:315-324.

24. Samnick S, Ametamey S, Leenders KL, Vontobel P, Quack G, Parsons CG, et al. Electrophysiological study, biodistribution in mice, and preliminary PET evaluation in a rhesus monkey of 1-amino-3-[18F]fluoromethyl-5-methyl-adamantane (18F-MEM): a potential radioligand for mapping the NMDA-receptor complex. Nucl Med Biol 1998; 25:323-330.

25. Shiue CY, Vallabhahosula S, Wolf AP, Dewey SL, Fowler JS, Schlyer DJ, et al. Carbon-11 labelled ketamine-synthesis, distribution in mice and PET studies in baboons. Nucl Med Biol 1997; 24:145-150.

26. Bowery NG, Wong EH, Hudson AL. Quantitative autoradiography of [3H]-MK-801 binding sites in mammalian brain. Br J Pharmacol 1988; 93:944-954.

27. Hartvig P, Valtysson J, Antoni G, Westerberg G, Langstrom B, Ratti Moberg E, et al. Brain kinetics of (R)- and (S)-[N-methyl-11C]ketamine in the rhesus monkey studied by positron emission tomography (PET). Nucl Med Biol 1994; 21:927-934.

28. McGinnity CJ, Hammers A, Riano Barros DA, Luthra SK, Jones PA, Trigg W, et al. Initial Evaluation of 18F-GE-179, a Putative PET Tracer for Activated N-Methyl D-Aspartate Receptors. J Nucl Med 2014; 55:423-430.

29. Sakurai SY, Cha JH, Penney JB, Young AB. Regional distribution and properties of [3H]MK-801 binding sites determined by quantitative autoradiography in rat brain. Neuroscience 1991; 40:533-543.

30. Tacconi S, Ratti E, Marien MR, Gaviraghi G, Bowery NG. Inhibition of [3H]-(+)-MK 801 binding to rat brain sections by CPP and 7-chlorokynurenic acid: an autoradiographic analysis. Br J Pharmacol 1993; 108:577-582.

31. Borschel WF, Myers JM, Kasperek EM, Smith TP, Graziane NM, Nowak LM, et al. Gating reaction mechanism of neuronal NMDA receptors. J Neurophysiol 2012; 108:3105-3115.

32. Quarum ML, Parker JD, Keana JF, Weber E. (+)-[3H]MK-801 binding sites in postmortem human brain. J Neurochem 1990; 54:1163-1168.

33. Haradahira T, Okauchi T, Maeda J, Zhang MR, Kida T, Kawabe K, et al. A positron-emitter labeled glycine(B) site antagonist, [(11)C]L-703,717, preferentially binds to a

cerebellar NMDA receptor subtype consisting of GluR epsilon3 subunit in vivo, but not in vitro. Synapse 2002; 43:131-133.

34. Erlandsson K, Bressan RA, Mulligan RS, Gunn RN, Cunningham VJ, Owens J, et al. Kinetic modelling of [123I]CNS 1261--a potential SPET tracer for the NMDA receptor. Nucl Med Biol 2003; 30:441-454.

35. Roussel S, Pinard E, Seylaz J. The acute effects of MK-801 on cerebral blood flow and tissue partial pressures of oxygen and carbon dioxide in conscious and alpha-chloralose anaesthetized rats. Neuroscience 1992; 47:959-965.

36. Garzon J, Rodriguez-Munoz M, Sanchez-Blazquez P. Direct association of Mu-opioid and NMDA glutamate receptors supports their cross-regulation: molecular implications for opioid tolerance. Curr Drug Abuse Rev 2012; 5:199-226.

37. Rodriguez-Munoz M, Sanchez-Blazquez P, Vicente-Sanchez A, Berrocoso E, Garzon J. The mu-opioid receptor and the NMDA receptor associate in PAG neurons: implications in pain control. Neuropsychopharmacology 2012; 37:338-349.

38. Oh S, Kim JI, Chung MW, Ho IK. Modulation of NMDA receptor subunit mRNA in butorphanol-tolerant and -withdrawing rats. Neurochem Res 2000; 25:1603-1611.

39. Miyamoto Y, Yamada K, Nagai T, Mori H, Mishina M, Furukawa H, et al. Behavioural adaptations to addictive drugs in mice lacking the NMDA receptor epsilon1 subunit. Eur J Neurosci 2004; 19:151-158.

40. Christiaans JAM, Klein PJ, Metaxas A, Kooijman EJM, Schuit RC, Leysen JE, et al. Synthesis and preclinical evaluation of carbon-11 labelled N-((5-(4-fluoro-2-[11C]methoxyphenyl)pyridin-3-yl)methyl)cyclopentanamine as a PET tracer for NR2B subunit-containing NMDA receptors. Nucl Med Biol. 2014; epub ahead of print 10 May 2014; doi: 10.1016/j.nucmedbio.2014.04.131.

41. Murray F, Kennedy J, Hutson PH, Elliot J, Huscroft I, Mohnen K, et al. Modulation of [3H]MK-801 binding to NMDA receptors in vivo and in vitro. Eur J Pharmacol 2000; 397:263-270.

Tables

Table 1 Affinity values of PK-209 (IC_{50}/K_i) and slope of the inhibition curves (Hill coefficient, nH) for targets showing ≥50% inhibition of control specific binding in the primary screen assays.

	Target	IC_{50} (M)[a]	Ki (M)[b]	nH
1	Adrenergic alpha 1A	$6.2 \cdot 10^{-6}$	$3.1 \cdot 10^{-6}$	1.1
2	Muscarinic M1	$5.3 \cdot 10^{-6}$	$4.6 \cdot 10^{-6}$	1.0
3	Muscarinic M2	$4.2 \cdot 10^{-6}$	$2.9 \cdot 10^{-6}$	0.8
4	Opioid κ (KOP)	$7.5 \cdot 10^{-6}$	$5.0 \cdot 10^{-6}$	1.0
5	Opioid μ (MOP)	$2.8 \cdot 10^{-6}$	$1.2 \cdot 10^{-6}$	0.8
6	NMDA (PCP site)	$4.0 \cdot 10^{-8}$	$2.2 \cdot 10^{-8}$	1.5
7	sigma (1 and 2)	$2.2 \cdot 10^{-6}$	$1.8 \cdot 10^{-6}$	0.9
8	Ca^{2+} channel (L, verapamil site)	$4.1 \cdot 10^{-6}$	$2.0 \cdot 10^{-6}$	0.7
9	Na^{+} channel (site 2)	$5.2 \cdot 10^{-6}$	$4.6 \cdot 10^{-6}$	1.0

[a] IC_{50} is the concentration of PK-209 inhibiting 50% of reference radioligand binding to the target of interest, and was obtained in assay conditions as described in the Cerep catalogue (Cerep, Poitiers, France).

[b] K_i values were obtained by transforming IC_{50} values according to the Cheng & Prusoff equation. For the transformation, K_D values of the reference radioligands were measured in parallel experiments.

Table 2 V_T of [^{18}F]PK-209, at baseline and after the administration of MK-801 (0.3 mg/kg).

[a]REGION OF INTEREST		SUBJECT 1		SUBJECT 2		SUBJECT 3	
Brain Area	**Volume (cm^3)**	**Baseline V_T (mL/cm^{-3})**	**Blocked V_T (mL/cm^{-3})**	**Baseline V_T (mL/cm^{-3})**	**Blocked V_T (mL/cm^{-3})**	**Baseline V_T (mL/cm^{-3})**	**Blocked V_T (mL/cm^{-3})**
Frontal Lobe	5.1 ± 0.4	10.8	8.9	11.7	7.3	9.0	10.6
Occipital lobe	7.2 ± 0.8	8.8	7.9	10.9	6.7	12.9	14.0
Temporal lobe	3.7 ± 0.3	10.2	9.0	11.3	6.9	11.3	12.8
Striatum (Caudate&Putamen)	1.3 ± 0.1	11.3	9.3	12.2	7.1	15.2	16.2
Cerebellum	4.0 ± 0.1	10.4	7.7	10.6	6.4	13.5	14.9
Whole Brain	97.0 ± 2.5	10.1	9.6	11.3	6.9	13.2	15.2
Mean V_T in frontal, occipital, temporal lobes, the striatum and the cerebellum		10.3±0.4	8.6±0.3*	11.3±0.3	6.9±0.2*	12.4±1.1	13.7±1.0*

[a] Individual values from left and right ROIs were derived separately, and averaged within each subject before calculating mean±SEM values of V_T in each brain region.

* $P<0.05$ vs. baseline condition, Wilcoxon matched-pair tests.

Titles and legends to Figures

Figure 1 Chemical structure of [^{18}F]PK-209 [3-(2-chloro-5-(methylthio)phenyl)-1-(3-([^{18}F]fluoromethoxy)phenyl)-1-methylguanidine].

Figure 2 Fractions of the plasma ^{18}F activity of unchanged PK-209 and its metabolites as a function of time

Blood samples were collected at 5, 10, 15, 30, 60, 90 and 120 min after the administration of [^{18}F]PK-209. The mean percentage of plasma radioactivity attributable to parent [^{18}F]PK-209, polar, and non-polar metabolites during the 2 h scans was 19.2±0.5%, 75.0±0.5%, and 5.7±0.1%, respectively. Due to rapid metabolism, the 1 minus polar fraction was used as a surrogate of unchanged tracer. Results at each time-point are presented as the mean±SEM of the parent, polar and non-polar radioactivity fractions from 3 monkeys/scanning condition.

Figure 3 Mean decay- and metabolite-corrected [^{18}F]PK-209 plasma input function

Blood from the femoral artery was manually sampled at 5-10 s intervals for a period of 5 min, beginning simultaneously with an injection of [^{18}F]PK-209. The manual blood time-activity curve was calibrated using the radioactivity concentrations in the discrete blood samples. Parent plasma input functions were then calculated for each subject by multiplying the calibrated manual curve with the fits to the plasma/whole-blood radioactivity ratios and parent fractions. The plasma [^{18}F]PK-209 input function peaked at 37.8±4.2 s post-injection, and decreased to 10% of its peak value within 3 min, both under baseline and blocking conditions.

Figure 4 Decay-corrected time-activity curves of [^{18}F]PK-209 in different brain regions, at baseline and after treatment with MK-801

Regions-of-interest (ROIs) were automatically defined using the INIA19 template for the rhesus monkey brain. ROIs were projected onto the complete dynamic PET images in order to extract time-activity curves. Radioactivity concentrations were calculated separately in areas of the left and right hemisphere, and expressed as percentage of injected dose per cm^3 of tissue (%ID/cm^3). Individual values from left and right ROIs were averaged within each subject, before calculating mean±SEM values of radioactivity concentration **at the mid time-point of each frame**. The rank order of peak radioactivity concentration was striatum and cerebellum > occipital, temporal, and frontal lobes, under both baseline and blocking conditions. At baseline, the washout of [^{18}F]PK-209-derived radioactivity was slower from NMDAr-rich brain regions relative to the cerebellum. Pretreatment with MK-801 (0.3 mg/kg), 30 min before the administration of [^{18}F]PK-209 reduced the mean area under the time-activity curve from 2.31±0.07 at baseline to 1.97±0.04 %ID/cm^3·min. Peak uptake values were observed earlier than baseline during the blocking scans.

Figure 5 Total distribution volume (V_T) images (A) and whole-brain Logan plots (B) of [^{18}F]PK-209 for subject 1, at baseline and after the administration of MK-801

Dynamic PET scans from propofol-anaesthetised monkeys were acquired over a period of 120 min. Parametric images were generated using plasma-input Logan graphical analysis, and are presented through the transaxial plane from areas of the cortex to the cerebellum. Images have been smoothed by isotropic Gaussian filter of 2 mm at full width at half maximum. Brain regional V_T values were overall reduced compared with baseline for subjects 1 and 2, and increased for subject 3.

FIGURE 1

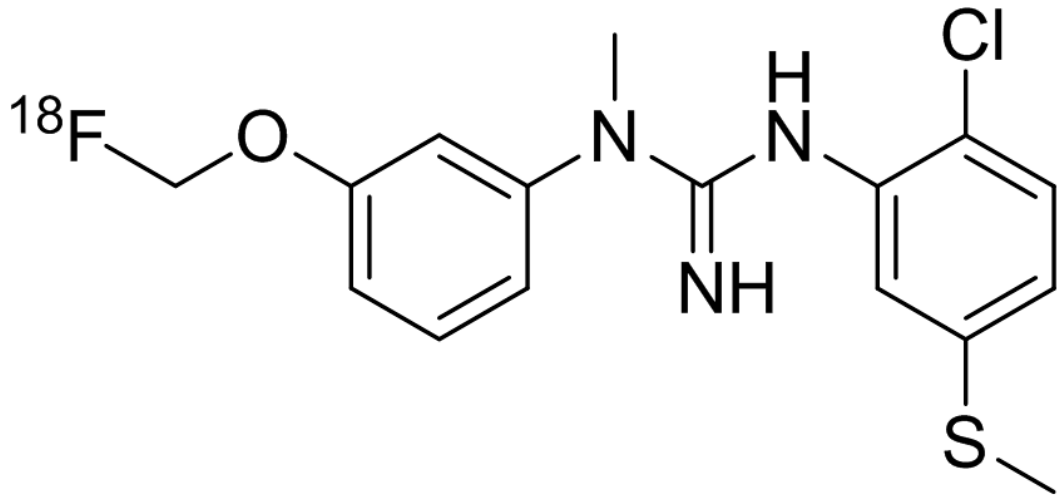

FIGURE 2

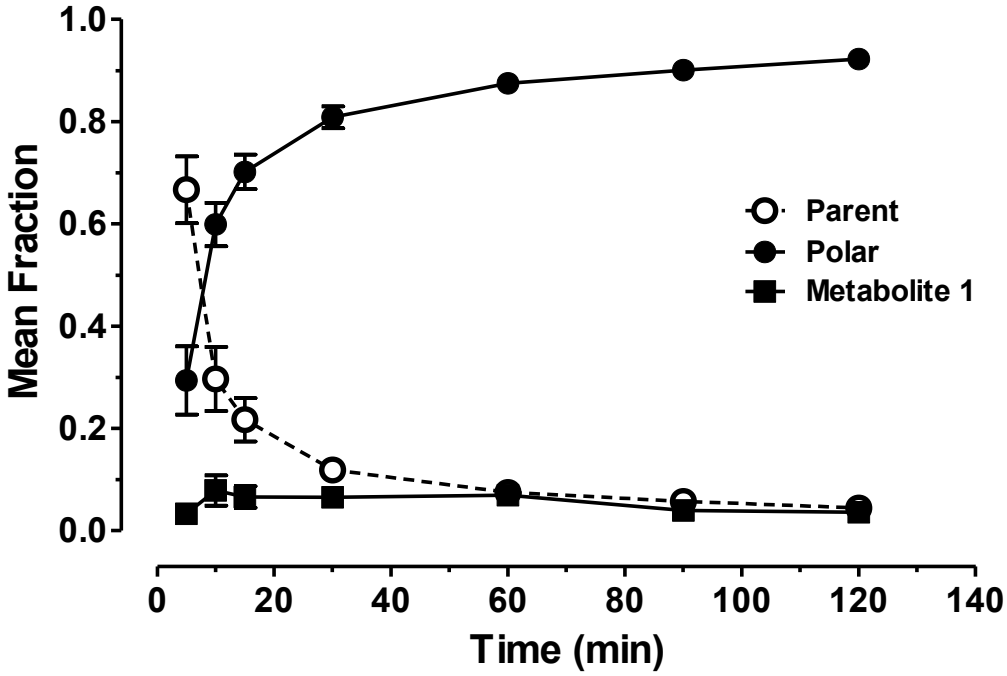
1.0
0.8
0.6
0.4
0.2
0.0
Mean Fraction
0
20
40
60
80
100
120
140
Time (min)
Parent
Polar
Metabolite 1

FIGURE 3

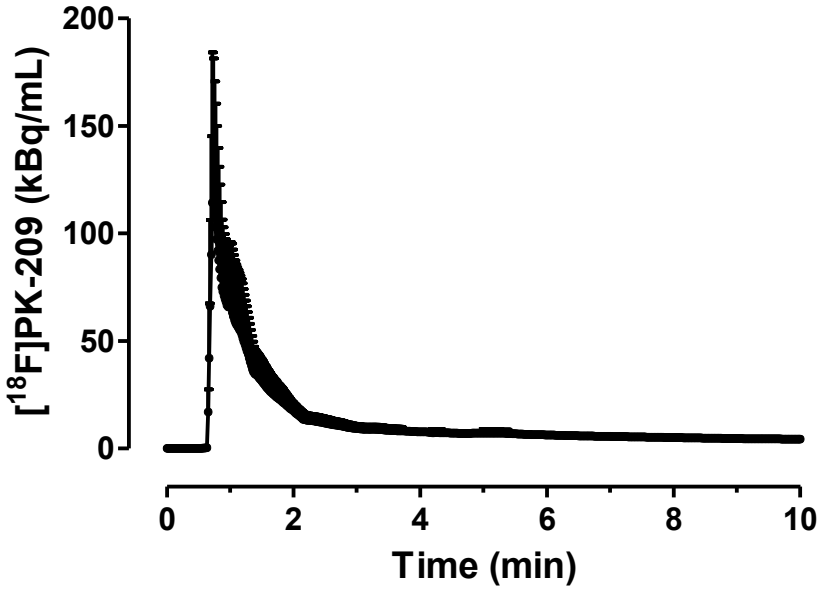

FIGURE 4

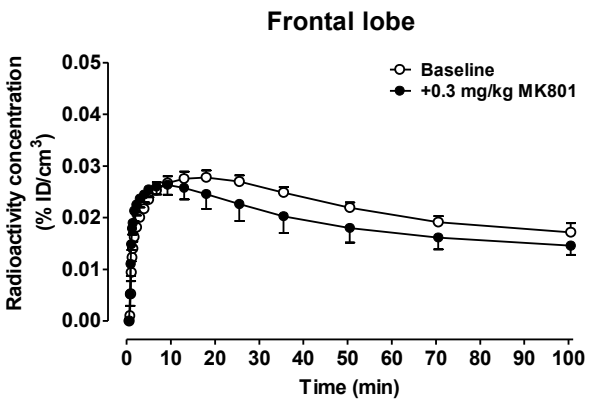
Frontal lobe
Baseline
+0.3 mg/kg MK801
Radioactivity concentration (% ID/cm3)
0.05
0.04
0.03
0.02
0.01
0.00
0 10 20 30 40 50 60 70 80 90 100
Time (min)

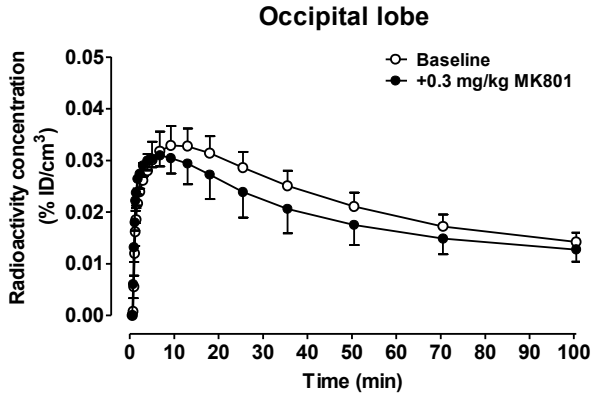
Occipital lobe
Baseline
+0.3 mg/kg MK801
Radioactivity concentration (% ID/cm3)
0.05
0.04
0.03
0.02
0.01
0.00
0 10 20 30 40 50 60 70 80 90 100
Time (min)

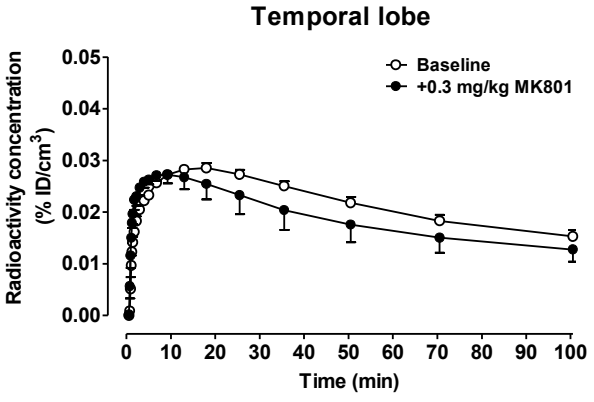
Temporal lobe
Baseline
+0.3 mg/kg MK801
Radioactivity concentration (% ID/cm3)
0.05
0.04
0.03
0.02
0.01
0.00
0 10 20 30 40 50 60 70 80 90 100
Time (min)

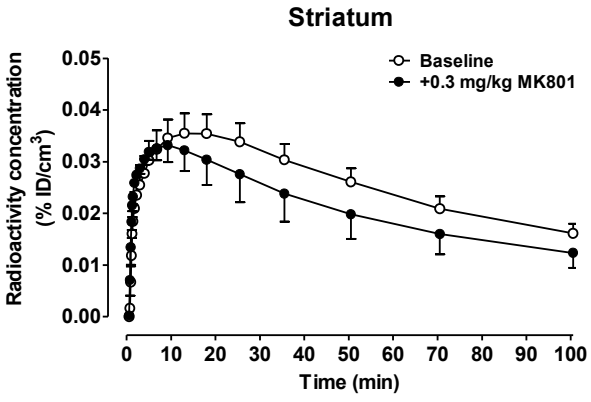
Striatum
Baseline
+0.3 mg/kg MK801
Radioactivity concentration (% ID/cm3)
0.05
0.04
0.03
0.02
0.01
0.00
0 10 20 30 40 50 60 70 80 90 100
Time (min)

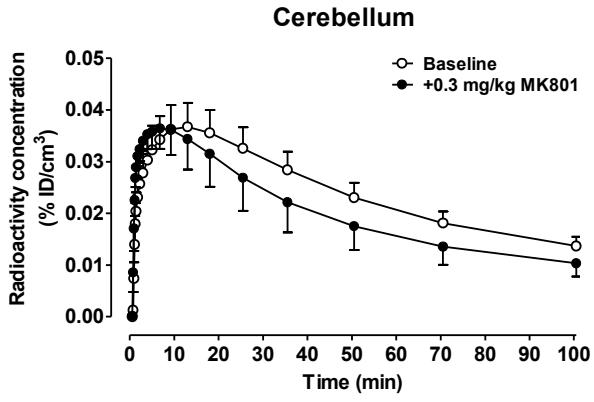
Cerebellum
Baseline
+0.3 mg/kg MK801
Radioactivity concentration (% ID/cm3)
0.05
0.04
0.03
0.02
0.01
0.00
0 10 20 30 40 50 60 70 80 90 100
Time (min)

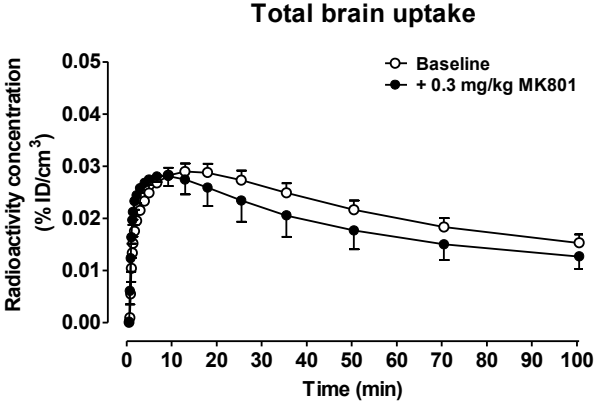
Total brain uptake
Baseline
+ 0.3 mg/kg MK801
Radioactivity concentration (% ID/cm3)
0.05
0.04
0.03
0.02
0.01
0.00
0 10 20 30 40 50 60 70 80 90 100
Time (min)

FIGURE 5

A

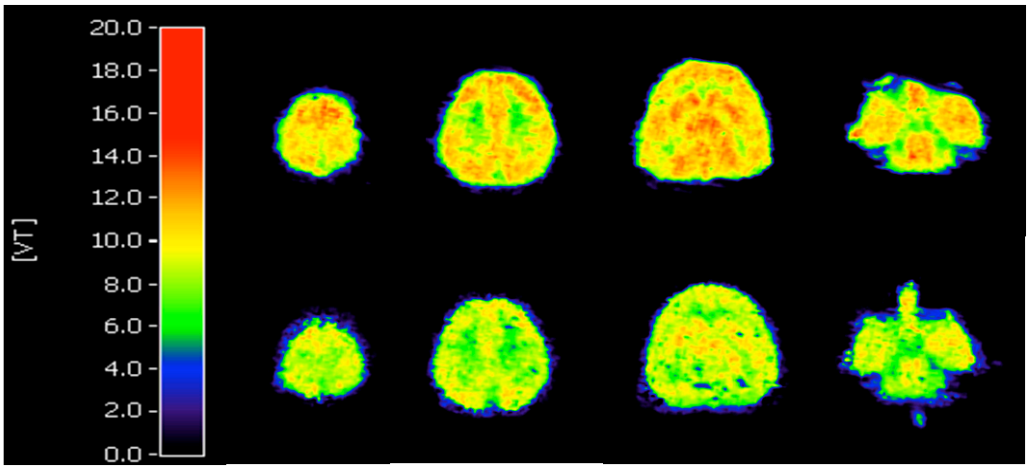
Baseline
+ MK-801
(0.3 mg/kg)
[VT]
20.0
18.0
16.0
14.0
12.0
10.0
8.0
6.0
4.0
2.0
0.0

B

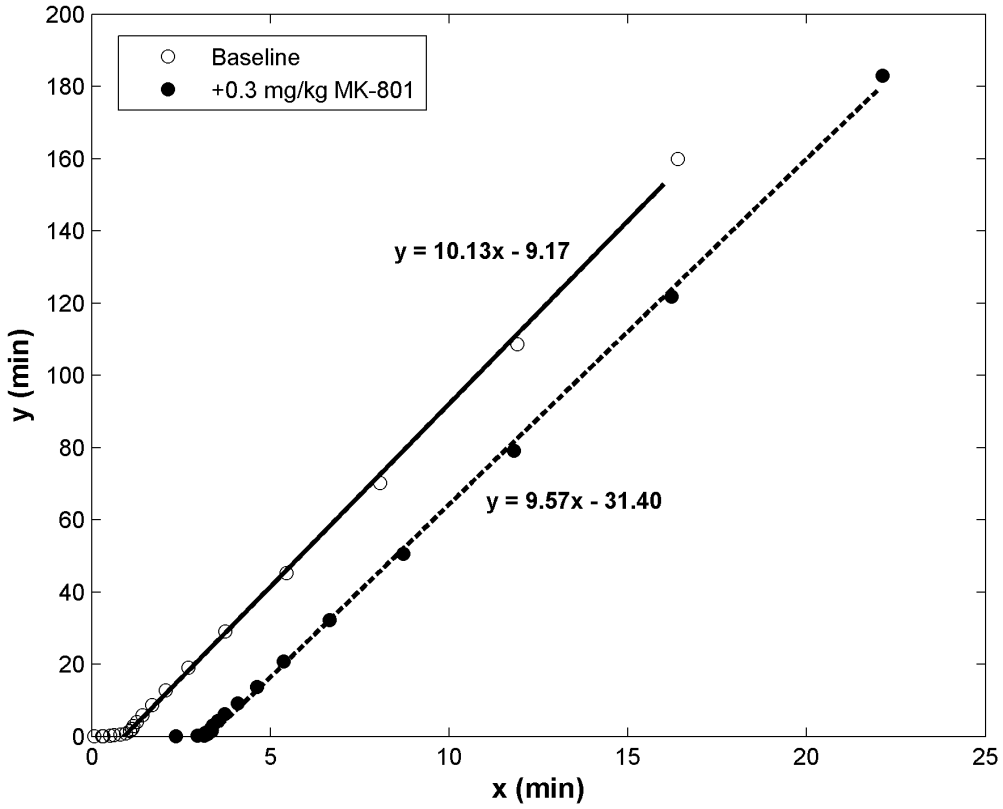
Baseline
+0.3 mg/kg MK-801
y = 10.13x - 9.17
y = 9.57x - 31.40
y (min)
x (min)
0
20
40
60
80
100
120
140
160
180
200
0
5
10
15
20
25